



ORIGINAL ARTICLE

Carbamohydrazone-thioate-based polymer-magnetic nanohybrids: Fabrication, characterization and bactericidal properties



Karolina H. Markiewicz^{a,*}, Iwona Misztalewska-Turkowicz^a, Katarzyna Niemirowicz^b, Robert Bucki^b, Anna M. Majcher^c, Agnieszka Z. Wilczewska^{a,*}

^a Institute of Chemistry, University of Białystok, Ciołkowskiego 1K, 15-245 Białystok, Poland

^b Department of Microbiological and Nanobiomedical Engineering, Medical University of Białystok, Mickiewicza 2c, 15-222 Białystok, Poland

^c Jagiellonian University, Faculty of Physics, Astronomy and Applied Computer Science, Prof. S. Łojasiewicza 11, 30-348 Cracow, Poland

Received 17 October 2016; accepted 19 December 2016

Available online 29 December 2016

KEYWORDS

Magnetic nanoparticles;
Polymer shell;
RAFT/MADIX polymerization;
Bactericidal properties

Abstract Herein is presented fabrication of new efficient antibacterial polymer/gold/magnetic nanohybrids. These nanohybrids consist of a superparamagnetic nanoparticle core, which ensures their facile separation, purification and recyclability, and polymeric coating which exhibits bactericidal activity. They were prepared in an efficient four-step synthetic route involving the following: (1) magnetic nanoparticles fabrication by co-precipitation of Fe^{2+} and Fe^{3+} in the presence of ammonia solution; (2) gold shell formation; (3) immobilization of RAFT/MADIX (reversible addition-fragmentation transfer/macromolecular design via the interchange of xanthates) initiating agent on the surface of nanoparticles; and (4) surface-initiated RAFT/MADIX polymerizations of bactericidal monomers. Physicochemical properties of bare and functionalized magnetic nanoparticles were characterized by Fourier transform infrared (FT-IR) spectroscopy, thermogravimetric analysis (TGA), magnetization measurements, transmission and scanning electron microscopies (TEM and SEM). Hemolytic and antibacterial activity of the obtained materials (monomers and polymer/gold/magnetic nanohybrids) against human red blood cells and *Pseudomonas aeruginosa* was determined. It was demonstrated that the tested agents do not affect red blood cells membrane permeability at the concentration range of 1–100 $\mu\text{g/ml}$. Simultaneously, at this concentration, they

* Corresponding authors.

E-mail addresses: k.markiewicz@uwb.edu.pl (K.H. Markiewicz), agawilcz@uwb.edu.pl (A.Z. Wilczewska).

Peer review under responsibility of King Saud University.



effectively kill and restrict metabolic activity of planktonic *P. aeruginosa* as well as prevent its biofilm formation.

© 2017 The Authors. Production and hosting by Elsevier B.V. on behalf of King Saud University. This is an open access article under the CC BY-NC-ND license (<http://creativecommons.org/licenses/by-nc-nd/4.0/>).

1. Introduction

Magnetic nanoparticles (MNPs) have been widely investigated in numerous applications, including microelectronics, catalysis and nanomedicine (Kainz and Reiser, 2014; Niemirowicz et al., 2012; Wilczewska and Misztalewska, 2014). In the biomedical field, research has mainly focused on the drug and gene delivery, hyperthermia and magnetic resonance imaging (Jiang et al., 2014; Kashevsky et al., 2015; Niemirowicz et al., 2012; Wilczewska et al., 2012). Recently, different studies suggested that some properties of nanoparticles such as resistance to biodegradation processes, surface activity and ability to penetrate bacteria cell membranes, could be beneficial in developing new methods for antibacterial treatment (Azam, 2012; Azam et al., 2012; Webster and Seil, 2012). Therefore, significant efforts have been made to develop nanosystems with antimicrobial activity (Dong et al., 2011; Webster and Seil, 2012; Webster and Taylor, 2011).

As bare MNPs tend to aggregate and phase separate in solutions, stabilization by appropriate surface modification is essential to assure they bioapplications. Magnetic nanoparticles may be covered with different materials e.g. gold or polymers (Jafari et al., 2010; Kainz and Reiser, 2014). Gold coating improves MNPs stability and biocompatibility, and it also enables their functionalization by organosulfur compounds (Moraes Silva et al., 2016). In turn, polymers ensure an efficient stabilization of nanoparticles and enable easy adjustment of chemical composition (homopolymer, copolymer) and properties (e.g. hydrophobic, hydrophilic) of a shell (Beija et al., 2011). Additionally, a suitably designed polymeric shell can offer other functions such as lower cytotoxicity, complexing properties or biological activity, leading to multifunctional nanosystems.

Herein formation of new antibacterial polymer/gold/iron oxide nanohybrids using surface-initiated RAFT/MADIX (reversible addition-fragmentation transfer/macromolecular design via the interchange of xanthates) polymerization method is described. In presented approach immobilization of RAFT/MADIX active species (chain transfer agents) on gold-coated magnetic cores is followed by surface-initiated polymerization. This way polymer chains are grown directly from the MNPs surface and high grafting density is achieved (Zhao and Perrier, 2015). The ability to control the thickness of polymeric shell by RAFT/MADIX method is demonstrated using commercially available monomer – styrene. Recently, we synthesized and fully characterized carbamohydrazonothioate-based monomers using thiosemicarbazide as starting material (Markiewicz et al., 2016; Bankiewicz et al., 2016). Thiosemicarbazide and certain of its derivatives (e.g. thiosemicarbazones) are known for their antimicrobial activity related to the ability to diffuse through semipermeable cell membranes (Bharti et al., 2003; Genova et al., 2004; Lobana et al., 2009; Sankaraperumal et al., 2013; Soykan and Erol, 2003). However, none of the reports concerns antibacterial properties of carbamohydrazonothioate derivatives or their polymeric nanohybrids with magnetic nanoparticles. Therefore, the obtained carbamohydrazonothioate-based monomers and carbamohydrazonothioate-based polymer-coated MNPs were tested in terms of their bactericidal properties. Magnetic nanocores covered with antibacterial polymeric shell are promising candidates as bactericidal agents that could be easily separated and reused. In our study we assess antibacterial activity of the obtained materials against *Pseudomonas aeruginosa*, an opportunistic pathogen responsible for different hospital infections. This pathogen frequently affects immunocompromised patients and those suffering from cystic fibrosis (de Bentzmann and Plésiat, 2011; Movahedi

et al., 2013). It is demonstrated that magnetic nanohybrids containing carbamohydrazonothioate-based polymers effectively kill and restrict metabolic activity of planktonic *P. aeruginosa* cells as well as cells embedded in a biofilm matrix. Furthermore, these nanosystems are characterized by low lytic activity against human red blood cells suggesting their biocompatibility.

2. Experimental section

2.1. Materials and methods

2-Mercaptoethanol, sulfuryl chloride, 2-bromopropionyl bromide, styrene, ethylenediamine, iron(III) chloride hexahydrate $\text{FeCl}_3 \cdot 6\text{H}_2\text{O}$, iron(II) chloride tetrahydrate $\text{FeCl}_2 \cdot 4\text{H}_2\text{O}$, and gold(III) chloride (HAuCl_4) solution were purchased from Sigma–Aldrich and used as received. Triethylamine was purchased from Avantor Performance Materials and was distilled before use. Initiator 2,2'-azobis(2-methylpropionitrile) (AIBN) was obtained from MERCK and was recrystallized from chloroform. All solvents were bought from Avantor Performance Materials and were distilled before use.

^1H and ^{13}C NMR spectra were recorded on a Bruker Avance spectrometer (400 and 100 MHz, respectively) as solutions in CDCl_3 , CD_3OD or DMSO. Chemical shifts are expressed in parts per million (ppm, δ) downfield from tetramethylsilane (TMS). FT IR spectra were recorded using Thermo Scientific Nicolet 6700 FT IR spectrophotometer. A thin layer of sample was placed in direct contact with an infrared attenuated total reflection (ATR) diamond crystal. All FT IR spectra were collected in the wave number range of $4000\text{--}500\text{ cm}^{-1}$ by co-adding 32 scans with a resolution of 4 cm^{-1} . TEM photographs and TEM/EDX analyses were done on Tecnai G2 X-TWIN transmission electron microscope. Energy-dispersive X-ray spectroscopy (EDX–detector Ametek Octane Pro) analyses were collected from the samples imaged by SEM (TFP 2017/12 Inspect S50 FEI). Samples for SEM microscopy were prepared on aluminum tables. Dynamic light scattering (DLS) was conducted using a Zetasizer Nano-ZS (Malvern Instruments, Ltd, UK) with integrated 4 mW He-Ne laser, $\lambda = 633\text{ nm}$. Thermogravimetric analyses (TGA) were performed on a Mettler Toledo Star TGA/DSC unit. Nitrogen was used as a purge gas (10 mL min^{-1}). Samples between 2 and 10 mg were placed in aluminum pans and heated from $25\text{ }^\circ\text{C}$ to $1000\text{ }^\circ\text{C}$ (TGA) with a heating rate of $10\text{ }^\circ\text{C/min}$. Magnetic properties of the nanoparticles were studied using a Quantum Design MPMS 5XL SQUID-type magnetometer. Each sample was placed in a standard gelatine capsule and immobilized with varnish glue for the measurement. All data were carefully corrected for the diamagnetic contribution of the holder.

Antimicrobial activity. Bioluminescent *Pseudomonas aeruginosa* Xen 5 strain (human septicaemia isolate which possesses a stable copy of the Photobacterium luminescens lux operon on the bacterial chromosome–PerkinElmer, USA) was used to evaluate antimicrobial activity and ability of tested agents to

prevent biofilm formation. Bacteria cells were cultured on Cetrymide agar at 37 °C for 24 h. The bactericidal activities of tested agents were measured using a killing assay and by monitoring changes of chemiluminescence intensity, which was performed using a Labsystems Varioscanner Lux (Thermo Scientific) according to previously published methods (Niemirówicz et al., 2015a). Activity of nanoparticles in comparison with free monomers against biofilm form was determined using spectrophotometric methods. To assess anti-biofilm activity crystal violet (CV) staining (0.1%) methods have been used. Briefly, biofilm of *P. aeruginosa* was grown for 48 h at 37 °C with and without the antibacterial agents (100 µg/ml). Each well was washed carefully with deionized water to remove planktonic bacteria. Then, 50 µl of crystal violet (0.1%) was added for 15 min. After incubation, excess stain was rinsed off with deionized water and dried. In next step 90 µl ethanol was added and optical density (OD) was determined at the wavelength of 570 nm. Hemolytic activity was investigated using human red blood cells (RBCs) suspended in phosphate-buffered saline (PBS) (hematocrit ~5%) with a concentration of tested antibacterial agents ranging from 0 to 100 µg/ml. RBCs were incubated with tested agents for 1 h at 37 °C. Relative hemoglobin concentration in supernatants after centrifugation at 2500 rpm for 15 min was monitored by measuring optical absorbance at 540 nm. 100% hemolysis was taken from samples in which 1% Triton X-100 was added to disrupt all cell membranes.

The hemolytic activity tests were performed under the Institutional Review Board (IRB) of the Medical University of Białystok approval (R-I-002/382/2012). IRB according to the Medical Profession Act of 5th December 1996 (Article 29.2) provides opinions on medical research projects taking into account the ethical criteria, and the advisability and feasibility of the project. All experiments were performed in compliance with the Polish Code of Medical Ethics (Chapter II "Research and biomedical experiments") and general principles of research ethics (the Helsinki Declaration, and Good Clinical Practice). The hemolytic activity of the tested agents was evaluated in blood samples from adult healthy volunteers. All subjects provided informed written consent and collected samples were anonymous.

2.2. Synthetic procedures

Synthesis of disulfanediylbis(ethane-2,1-diyl)bis(2-((ethoxy-carbono-thioyl)thio)propanoate) (DTC). 2,2'-Disulfanediylbis(ethane-1-ol) (1). 2-Mercaptoethanol (2.7 mL, 38.5 mmol, 2 equiv.) was dissolved in sulfuric chloride (1.6 mL, 19 mmol, 1 equiv.) and stirred for 10 min at room temperature. The excess of sulfuric chloride was removed under reduced pressure. The crude product was purified by silica gel chromatography (hexane/ethyl acetate v/v 6:4) to give pale yellow oil (1.57 g, 54%); ¹H NMR δ_H (400 MHz, CDCl₃): 3.89 (4H, t, J = 5.9), 2.88 (4H, t, J = 5.9); ¹³C NMR δ_C (100 MHz, CDCl₃): 60.3 (—CH₂—O—), 41.2 (—CH₂—S—); FT IR ν_{max} (CHCl₃): 3412 (O—H), 2931, 2879 (C—H), 1465 (C—H), 1402 (O—H), 1056 (C—O).

Disulfanediylbis(ethane-2,1-diyl) bis(2-bromopropanoate) (2). 2-Bromopropionic acid (2 mL, 18.8 mmol, 2 equiv.) was added dropwise to a solution of compound 1 (1.45 g, 9.4 mmol, 1 equiv.) and triethylamine (2.6 mL, 18.8 mmol) in

dry dichloromethane (10 mL). The mixture was stirred at room temperature under argon gas protection for 8 h. Next, the reaction was quenched with water and the mixture was extracted with dichloromethane. The organic phases were washed with 5% K₂CO₃ and water, dried over anhydrous sodium sulfate, and concentrated under reduced pressure. The crude product was purified by silica gel chromatography (hexane/ethyl acetate v/v 9:1) to give yellow oil 2 (1.92 g, 48%); ¹H NMR δ_H (400 MHz, CDCl₃): 4.43–4.34 (6H, m, —CH—C(O)—, —CH₂—O—), 2.95 (4H, t, J = 7.0, —CH₂—S—), 1.81 (6H, d, J = 7.0); ¹³C NMR δ_C (100 MHz, CDCl₃): 169.9 (—C(O)—), 63.4 (—CH₂—O—), 39.7 (—CH—), 36.6 (—CH₂—S—), 21.5 (—CH₃); FT IR ν_{max} (CHCl₃): 2930, 2890 (C—H), 1740 (C=O), 1157 (C—O), 1074 (C—O).

Disulfanediylbis(ethane-2,1-diyl) bis(2-(ethoxycarbono-thioyl)thio) propanoate (3). Potassium ethyl xanthate (1.35 g, 8.6 mmol, 2 equiv.) was gradually added to the solution of compound 2 (1.8 g, 4.3 mmol, 1 equiv.) in acetone (20 mL). The reaction mixture was stirred for 30 min at 0 °C. White powder which precipitated in the course of the reaction was filtered and next, extracted with water and dichloromethane. The organic phases were dried over anhydrous sodium sulfate, and concentrated under reduced pressure to afford 2.96 g (83%) of yellow oil 3; ¹H NMR δ_H (400 MHz, CDCl₃): 4.65–4.59 (2H, k, J = 7.1, —CH₂—O—), 4.40–4.35 (6H, m, —CH—C(O)—, —CH₂—O—), 2.92 (2H, t, J = 6.5, —CH₂—S—), 1.56 (3H, d, J = 7.4, —CH₃), 1.40 (3H, t, J = 7.1, —CH₃); ¹³C NMR δ_C (100 MHz, CDCl₃): 211.8 (—C(S)—), 171.1 (—C(O)—), 70.2 (—CH₂—), 63.2 (—CH₂—O—), 46.7 (CH), 36.8 (—CH₂—S—), 16.7 (—CH₃), 13.6 (—CH₃); FT IR ν_{max} (CHCl₃): 2961, 2939, 2874 (C—H), 1736 (C=O), 1227 (C—S), 1047(C=S).

Synthesis of MNP@Au-DTC (MNP-6). Iron oxide nanoparticles (MNP-4) were synthesized according to the published method (Wilczewska and Markiewicz, 2014). Au coating procedure (MNP@Au-5) was carried out in an ultrasound bath, according to the known method (Tamer et al., 2010). MNP@Au particles (0.4 g) were suspended in methanol (25 mL). Next, the solution of DTC (0.2 g) in dichloromethane (10 mL) was added dropwise. The resulting mixture was stirred for 24 h. MNP@Au-DTC particles were separated by magnetic decantation, washed twice with methanol and dichloromethane and dried into powder at 60 °C. ATR FTIR ν_{max}: 3343 (O—H), 2920 (C—H), 1728 (C=O), 1367 (C—N), 1218 (C—H), 1044 (C=S), 546 (Fe—O).

General procedure for RAFT/MADIX polymerization on MNP@Au-DTC. A typical polymerization procedure was as follows: the mixture of MNP@Au-DTC, monomer, solvent and initiator was sonicated until a homogeneous suspension was formed. The dispersion was degassed by bubbling argon for 15 min, and then, the mixture was transferred into an oil bath with a constant temperature. Polymerization was stopped by diluting the mixture in solvent (toluene, THF, methanol) and magnetic decantation. The cycle of redispersion and magnetic separation was repeated several times to rinse free polymer chains and obtain 'pure' polymer-grafted nanoparticles. MNP@Au-PS ATR FTIR ν_{max}: 3058, 3024 (C_{Ar}—H), 2916, 2847 (C—H), 1599, 1490, 1448 (C=C), 1067 (C=S), 693 (C—H), 546 (Fe—O). MNP@Au-PBM ATR FTIR ν_{max}: 3024 (C_{Ar}—H), 2921 (C—H), 1603 (NH), 1410 (CH), 1327 (C—N), 839 (N—H), 726 (C—S), 692 (C_{Ar}—H), 559 (Fe—O).

MNP@Au-PBMS ATR FTIR ν_{\max} : 3019 ($C_{Ar}-H$), 2911 ($C-H$), 1666, 1605, 1507 ($N-H$), 1418 ($C-H$), 1325 ($C-N$), 828 ($N-H$), 691 ($C_{Ar}-H$), 559 ($Fe-O$). MNP@Au-PBM_2 ATR FTIR ν_{\max} : 3054 ($C_{Ar}-H$), 2918 ($C-H$), 1603, 1544 ($N-H$), 1404 ($C-H$), 1326 ($C-N$), 1235, 1017 ($C-H$), 843 ($N-H$), 725 ($C-S$), 691 ($C_{Ar}-H$), 554 ($Fe-O$). MNP@Au-PBM-*r*-PS ATR FTIR ν_{\max} : 3056 ($C_{Ar}-H$), 2908 ($C-H$), 1605, 1549 ($N-H$), 1445 ($C=C$), 1397 ($C-N$), 1205, 1015 ($C-H$), 840 ($N-H$), 720 ($C-S$), 689 ($C_{Ar}-H$), 547 ($Fe-O$).

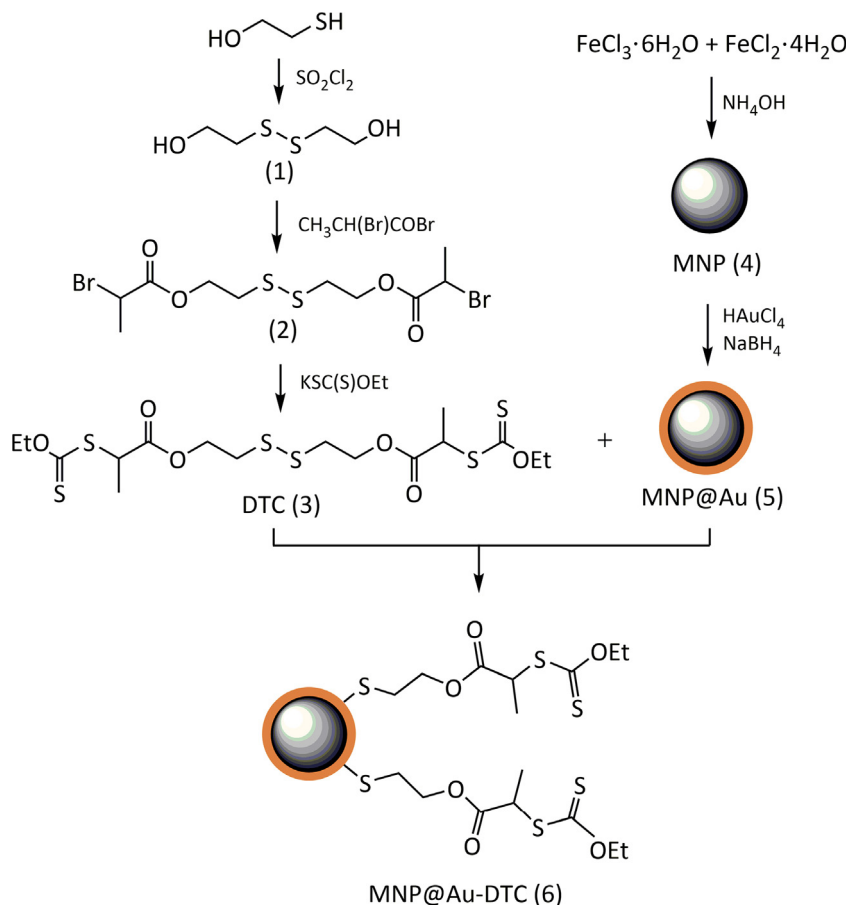
3. Results and discussion

Synthesis of RAFT/MADIX chain transfer agent. RAFT/MADIX technique is a type of controlled radical polymerization which uses xanthates/dithiocarbonates to mediate polymerization process (Destarac et al., 2002; Taton et al., 2001). In this study, RAFT/MADIX chain transfer agent – dithiocarbonate 3 – was obtained in a simple and efficient synthetic way presented in Scheme 1. Initially, the reaction of 2-mercaptoethanol with sulfonyl chloride gave compound 1 in yield 54%. Next, esterification of diol 1 with 2-bromopropionic acid bromide provided product 2 (48%). The reaction of bromoester 2 with potassium ethyl xanthate led to the formation of dithiocarbonate 3 (DTC) in a high yield (83%) (Supporting material, Figs. S1–S3).

Immobilization of dithiocarbonate 3 on MNP@Au. The formation of MNP@Au-DTC involved three steps: iron oxide

cores synthesis (MNP-4), gold coating (MNP@Au-5), and immobilization of RAFT/MADIX chain transfer agent (MNP@Au-DTC-6). Iron oxide nanoparticles were synthesized according to the well-established method by coprecipitation of Fe^{2+} and Fe^{3+} (in the molar ratio of 1:2) in the presence of 25% NH_4OH solution (Wilczewska and Markiewicz, 2014). Gold shell around magnetic cores was obtained using the most common procedure *i.e.* reduction of $HAuCl_4$ by sodium borohydride (Tamer et al., 2010). Immobilization of DTC 3 on gold-coated MNPs was achieved by chemisorption (Scheme 1). Organosulfur compounds bind strongly to gold surfaces forming self-assembled monolayers (SAMs) (Rudolf et al., 2011). The reactivity of alkanethiols and di-*n*-disulfides toward gold has been thoroughly studied (Bain et al., 1989; Ulman, 1996). Although they form undistinguishable SAMs on gold, the mechanism of their chemisorption is different and disulfides show lower activation barrier for adsorption than thiols. Chemisorption of thiols involves *e.g.* breaking of the $S-H$ bond and formation of the $H-Au$ bonds, $H-H$ bonds, whereas disulfide chemisorption requires only cleavage of the $S-S$ bond and formation of two thiolate-gold bonds (Lavrich et al., 1998). Fenter et al. reported that disulfides may chemisorb as dimers without dissociation (Fenter et al., 1994).

Bare and functionalized MNPs were characterized by several methods including transmission electron microscopy (TEM), scanning electron microscopy (SEM), energy disper-



Scheme 1 Synthesis of RAFT/MADIX chain transfer agent – dithiocarbonate (DTC) and its immobilization on gold-coated MNPs.

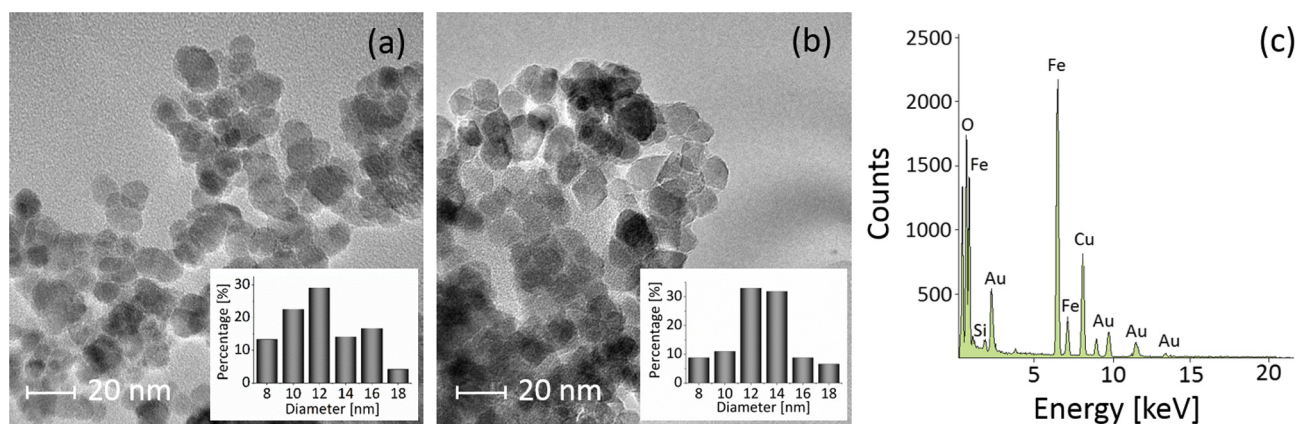


Figure 1 TEM images of (a) bare and (b) gold-modified MNPs (insets show histograms of the diameter distribution), (c) TEM/EDX spectrum of MNP@Au nanoparticles.

sive X-ray analysis (EDX), X-ray powder diffraction (XRPD), Fourier transform infrared (FT-IR) spectroscopy, and thermogravimetric analysis (TGA).

Iron oxide nanoparticles are likely to agglomerate and in TEM micrographs aggregates of magnetic cores are observed (Fig. 1). Particles were found to be spherical with a relatively narrow size distribution and an average size of $\sim 12 (\pm 2)$ nm and $\sim 13 (\pm 2)$ nm for MNPs (Fig. 1a) and MNP@Au (Fig. 1b), respectively. The average size of magnetic nanoparticles was determined by measuring the diameter of 100–200 particles on TEM images. No difference in mean particle size was observed after DTC chemisorption (Supporting material, Fig. S4). The atomic composition of modified magnetic nanoparticles was determined using energy dispersive X-ray (EDX) method. TEM/EDX analysis confirmed the presence of gold in MNP@Au sample (3.60%). It is worth nothing that gold in the form of nanoparticles was very rarely observed in TEM grid. Furthermore, results of SEM/EDX analysis of MNP@Au particles showed that the sample is relatively homogeneous. Taking this into consideration, it was concluded that gold is present at the MNPs surface in the form of a layer. In MNP@Au-DTC specimen, gold (2.48%) and sulfur (0.93%) were detected by TEM/EDX analysis (Supporting material, Table S1).

The phase composition of MNPs and MNP@Au samples was investigated by X-ray powder diffraction (Supporting material, Fig. S5). In the diffractograms of both samples, typical set of signals of magnetite/maghemite ($\text{Fe}_3\text{O}_4/\gamma\text{-Fe}_2\text{O}_3$) [(220), (311), (400), (422), (511), (440)] (Kalska-Szostko et al., 2015; Mahadevan et al., 2007) can be seen. In MNP@Au diffractogram the crystalline structure of metallic gold is also observed (111), (200), (220), (311) (Robinson et al., 2010).

A set of ATR FT-IR spectra of bare and modified MNPs is presented in Fig. 2a. In each spectrum, the presence of the magnetic core is indicated by broad band at 550 cm^{-1} which corresponds to the Fe-O stretching modes. No substantial changes were observed after gold coating step, whereas strong modification of IR signals occurred after DTC immobilization. In the latter case, the peaks at 1218 cm^{-1} and at 1044 cm^{-1} can be assigned to the C—O—C and C=S stretching vibrations of ethyl dithiocarbonate groups. The absorption mode at 1728 cm^{-1} corresponds to the vibrations of carbonyl ester group and the band around 2920 cm^{-1} to C—H stretching modes of DTC. Fig. 2b presents thermograms of MNP, MNP@Au, and MNP@Au-DTC. The TG curve of bare MNPs shows a small weight loss (5%), most likely related to removal of adsorbed solvents. Lower total weight loss (3%) is observed for MNP@Au sample due to the gold residuals.

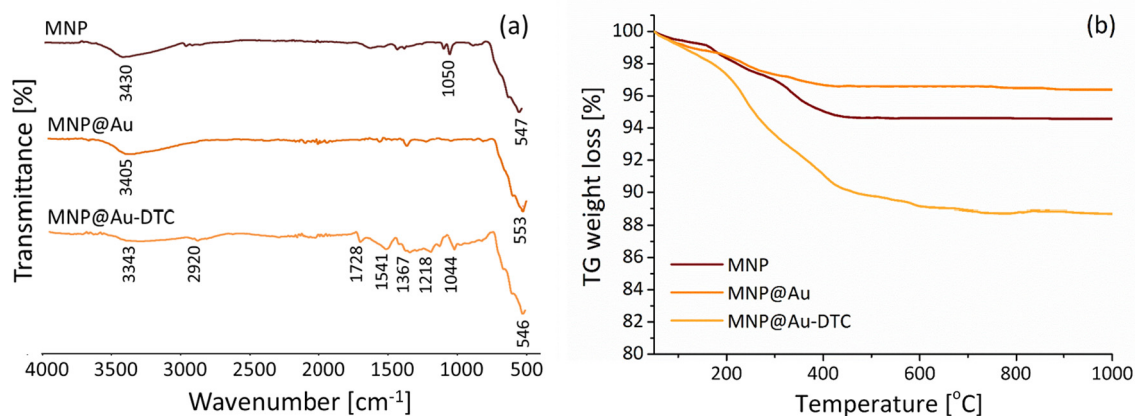
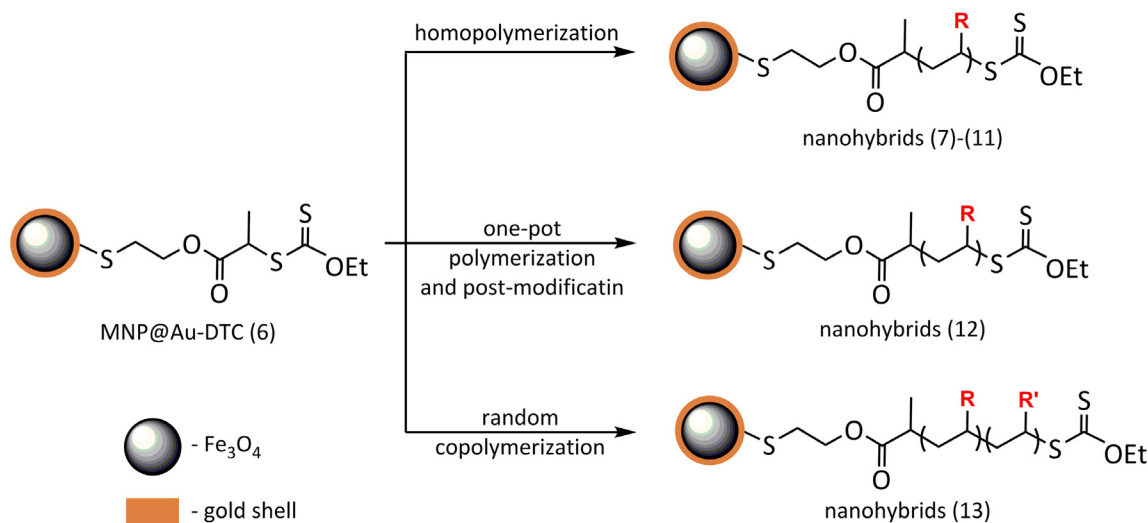


Figure 2 (a) ATR FT IR spectra and (b) TG curves of bare and modified MNPs.



Scheme 2 Formation of polymeric shells on DTC-coated MNP@Au.

The TG curve of MNP@Au-DTC shows 10% of a total weight loss indicating the presence of additional component (dithiocarbonate) on magnetic nanoparticles surface.

Surface-initiated RAFT/MADIX polymerization on MNP@Au-DTC. Immobilization of dithiocarbonate on gold-coated MNPs was followed by surface initiated RAFT/MADIX polymerizations of various vinyl monomers (Scheme 2, Table 1, Table S2). RAFT/MADIX technique enables to control growth, composition and architecture of polymers (Perrier and Takolpuckdee, 2005). It can be easily performed in mild conditions and is compatible with a huge variety of monomers (Beija et al., 2011; Destarac, 2010; Perrier and Takolpuckdee, 2005). In the presented approach dithiocarbonates are anchored to a nanoparticle surface by their R-group and consequently act as propagating leaving groups during polymerization. This way polymer chains are grown directly from a nanoparticle surface. Polymerization reactions were performed by introduction of a dithiocarbonate-coated magnetic nanoparticles (MNP@Au-DTC) to a conventional free-radical system (monomer, solvent and initiator). Prior to each reaction RAFT/MADIX agent, monomer, and solvent were sonicated until a homogeneous suspension was formed. 2,2'-Azobis(2-methylpropionitrile) (AIBN) was used as initiator and toluene or ethanol as solvents. As formation of polymer chains in solution is unavoidable, a cycle of redispersion in solvent and magnetic separation was used several times to rinse free polymer chains and unreacted monomer and to obtain 'pure' polymer-grafted nanoparticles.

Initially, to demonstrate the ability to control the thickness of polymeric shell on MNP@Au-DTC using RAFT/MADIX method, polymerizations of commercially available styrene were conducted with various times of reaction (2, 6, 24 h). The ATR FT-IR spectra of obtained polymer-magnetic nano hybrids are presented in Fig. 3a. The spectra clearly indicate the presence of polystyrene at the surface of MNP@Au. The peaks at characteristic frequencies corresponding to vibrations of polystyrene chains (3024, 2920, 1599, 1490, 1448 and 695 cm^{-1}) are observed. Additionally, the intensity ratio of

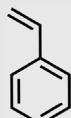
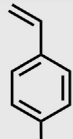
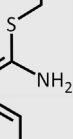
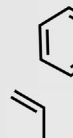
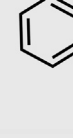
polystyrene to magnetic core bands increases with the reaction time indicating thicker polymeric layer.

Fig. 3b and d show thermograms of polystyrene-magnetic nanoparticles obtained with various reaction time. TG/DTG curves present one-stage weight loss in temperature range of 400–450 °C and the maximum at 420 °C attributed to the degradation of polystyrene chains. It can be observed that the amount of polymer grafted to the MNPs increases with the reaction time. TG curves of MNP@PS particles 7, 8, and 9 show a total weight loss of 54%, 44% and 18%, respectively, which can be roughly estimated as the weight of polystyrene grafted on MNPs surface. The results of FT IR and TG/DTG analyses indicate dependence of the polymer chains length on the duration of reaction and confirm ability to control thickness of polymeric shell around MNPs. Additionally, polymerization of styrene in the presence of MNP@Au was carried out. This simple experiment proved that formation of polymeric shell is inherently related to dithiocarbonates chemisorbed on MNP@Au as no polymer shell was observed in MNP@Au case.

Magnetization versus field curves were measured within a range of temperatures. For all of the samples it was necessary to increase the temperature up to the experimentally available maximum of 400 K to approach the superparamagnetic region and to obtain closing of the hysteretic loops that were still visible at 300 K. Law of approach to saturation (LA) was fitted to the data in high magnetic fields to obtain the values of the saturation magnetization (Abbas et al., 2013; Guivar et al., 2014). As can be clearly seen for the polystyrene-coated nanoparticles, increasing the time of the reaction (*i.e.* increasing the thickness of the polymeric shell) causes reduction in the saturation magnetization value from 69.61 emu/g for bare nanoparticles down to 50.14, 45.65, and 39.19 emu/g after 2, 6, and 24 h of polymerization, respectively.

X-ray powder diffraction performed for chosen polymer-magnetic nano hybrids (Supporting material, Fig. S5) showed typical signals of magnetite/maghemite and metallic gold. These results suggest preservation of the core crystal structure after polymerization.

Table 1 Summary of polymeric shells built on MNP@Au-DTC.

Type of polymerization	Type of monomer	Nanohybrids	TG weight loss [%]
Homopolymerization		MNP@Au-PS_24 h (7) MNP@Au-PS_6 h (8) MNP@Au-PS_2 h (9)	54 44 18
		MNP@Au-PBM (10)	30
		MNP@Au-PBMS (11)	40
One-pot polymerization and post-modification		MNP@Au-PBM_2 (12)	41
		MNP@Au-PBM- <i>r</i> -PS (13)	23

In the next step, in order to prepare multifunctional polymer-magnetic nanohybrids with antibacterial activity, polymerizations of original vinyl monomer obtained from thiosemicarbazide were performed on MNP@Au-DTC (Table 1). The synthesis and full characterization of monomer have been recently reported (Markiewicz et al., 2016). Three types of polymerization were performed: homopolymerization (MNP-10, MNP-11), one-pot homopolymerization and modification (MNP-12), and random copolymerization (MNP-13) (Scheme 2, Table 1). Homopolymerizations were performed for carbamohydrazone-thioate-based monomer (MNP@Au-PBM) and its hydrochloric salt (MNP@Au-PBMS) that can be polymerized in less toxic polar solvents (e.g. ethanol). This kind of polymerization introduces large amount of functional groups on the surface of MNPs. Due to the possibility of steric hindrance, random copolymer with styrene as comonomer was prepared (MNP@Au-PBM-*r*-PS). Additionally, one-pot polymerization of 4-vinylbenzyl chloride with simultaneous modifi-

cation of chloride with benzaldehyde thiosemicarbazone was performed. The influence of the method of shell preparation on physicochemical properties of nanohybrids was investigated.

After reactions, changes in FT-IR spectra of all samples in comparison with MNP@Au-DTC spectrum are observed, primarily, in the fingerprint region (Fig. 4a). At 690 cm^{-1} C–H bending vibrations of aromatic rings are present. Additional bands around $1200\text{--}1450\text{ cm}^{-1}$ that can be ascribed to vibrations of CH and CH_2 groups in polymer chains are present. The stretching modes of C=N, and $\text{C}=\text{C}_{\text{Ar}}$ groups showed up at $1500\text{--}1600\text{ cm}^{-1}$ with various intensity and shape depending on way of shell preparation. Stretching vibrations of polymeric CH, CH_2 groups and aromatic C–H bonds are observed around 2920 cm^{-1} and 3020 cm^{-1} , respectively.

Thermogravimetric studies were performed to investigate thermal properties of the obtained nanohybrids (Fig. 4b and d). After polymerizations total weight loss in all

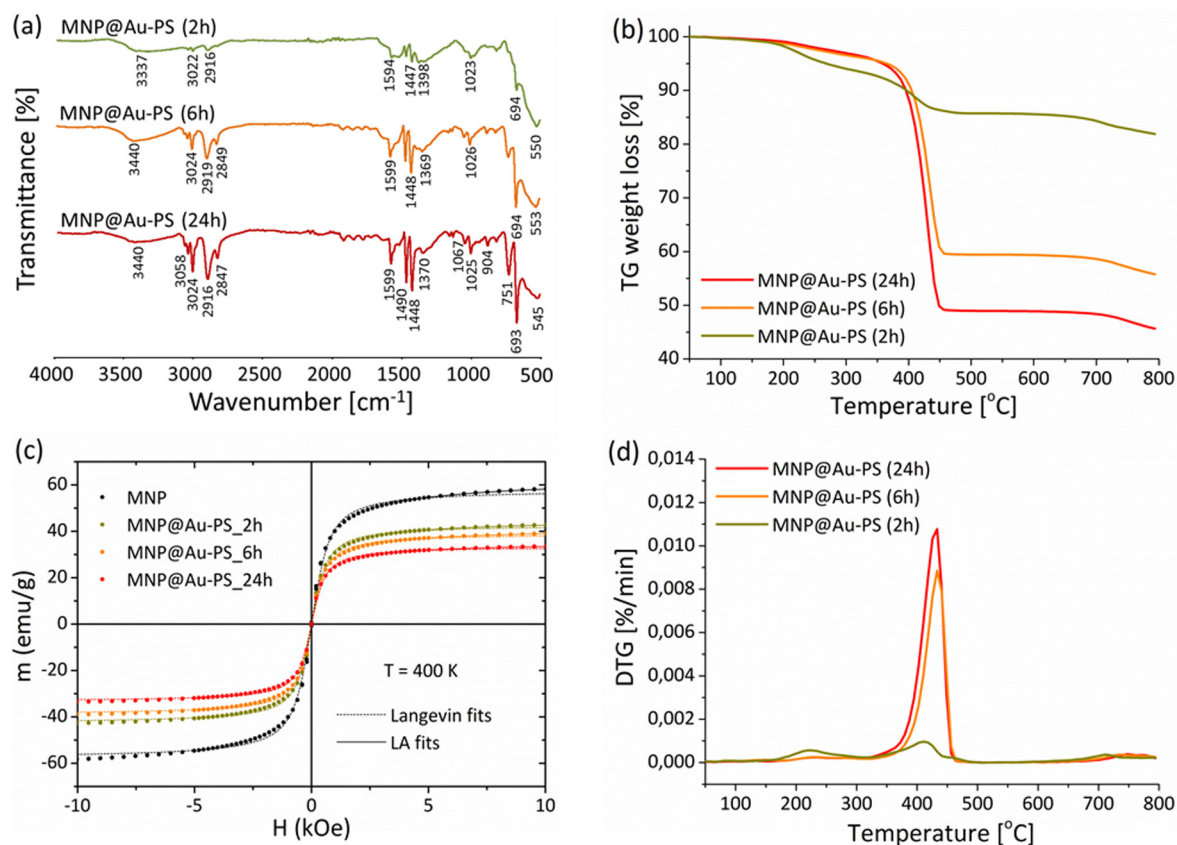


Figure 3 (a) ATR FT-IR spectra; (b) TGA curves; (c) magnetization as a function of external magnetic field measured at 400 K; and (d) DTG curves of polystyrene-coated magnetic nanoparticles.

samples is higher than for MNP@Au-DTC (30% for MNP@Au-PBM, 40% for MNP@Au-PBMS, 41% for MNP@Au-PBM_2, and 23% for MNP@Au-PBM-*r*-PS). In the thermograms of all samples similar curves characteristics can be observed. TG and DTG curves show three stages of weight loss at temperature ranges of 200–300 °C, 300–500 °C and 700–850 °C. The first two ones, with the maxima around 280 °C and 400 °C are most likely related to the decomposition of carbamohydranothioate part, whereas the third one, with the maximum at 800 °C, is attributed to the degradation of the polymer chain.

Magnetization measurements of the samples showed similar dependence as for the polystyrene-grafted MNP. The M_S values observed for polymer-coated MNP are much lower comparing to the M_S of bare MNPs. For the samples MNP@Au-PBM and MNP@Au-PBMS the M_S value is 36.72 and 20.34 emu/g at 300 K, respectively, and for the samples MNP@Au-PBM-*r*-PS and MNP@Au-PBM_2 it is equal to 33.85 and 25.34 emu/g. These results are consistent with our previous studies which revealed that M_S value mostly depends on the thickness of a shell and barely depends on its composition (Misztalewska et al., 2015).

Fig. 5 presents TEM and SEM images of MNP@Au-PBM particles. The shell surrounding MNP@Au core is easily observable in TEM micrograph. SEM picture shows granular texture of the material. Similar morphologies were observed in cases of other nanohybrids; however, the shell thickness varies, depending on the polymer preparation method (Supporting material, Fig. S6).

DLS analysis taken for selected samples (MNP, MNP@Au-DTC, MNP@Au-PBM, MNP@Au-PBMS) showed that covering nanoparticles with Au, DTC and PBM shells leads to decrease in their hydrodynamic size (Supporting material, Fig. S7). It can be explained by the fact that bare nanoparticles exhibit a strong tendency for aggregation caused by their high surface area. Formation of covering layer around magnetic cores prevents agglomeration and thus smaller aggregates are detected by DLS. In the case of MNP@Au-PBMS sample the measured hydrodynamic size is comparable to the value obtained for bare MNP. The effect of aggregation in this case may be related to the chemical nature of the shell (PBMS is hydrochloric salt of PBM). Zeta potential measurements show that synthesis of polymeric layers on magnetic cores leads to formation of more stable particles.

Biological studies. Different mechanisms of MNPs action against bacteria were described such as generation of reactive oxygen species (ROS), interference with bacterial electron transport of oxidation of NADH, membrane disruption, and damage of macromolecules (DNA, lipids and protein) (Niemirowicz et al., 2015b; Thomas Webster, 2010; Webster et al., 2013). However, observed divergent effects of nanoparticles against bacteria cell might be linked with dose, nature of nanomaterial coating, external factors and type of bacteria strain (Hajipour et al., 2012; Webster and Taylor, 2011; Ashkarran et al., 2012). In our study, the potential of bifunctional monomers (BM and BMS), and chosen polymer-magnetic nanohybrids (MNP-8, MNP-10, MNP-11 and MNP-12) against *Pseudomonas aeruginosa* was investigated.

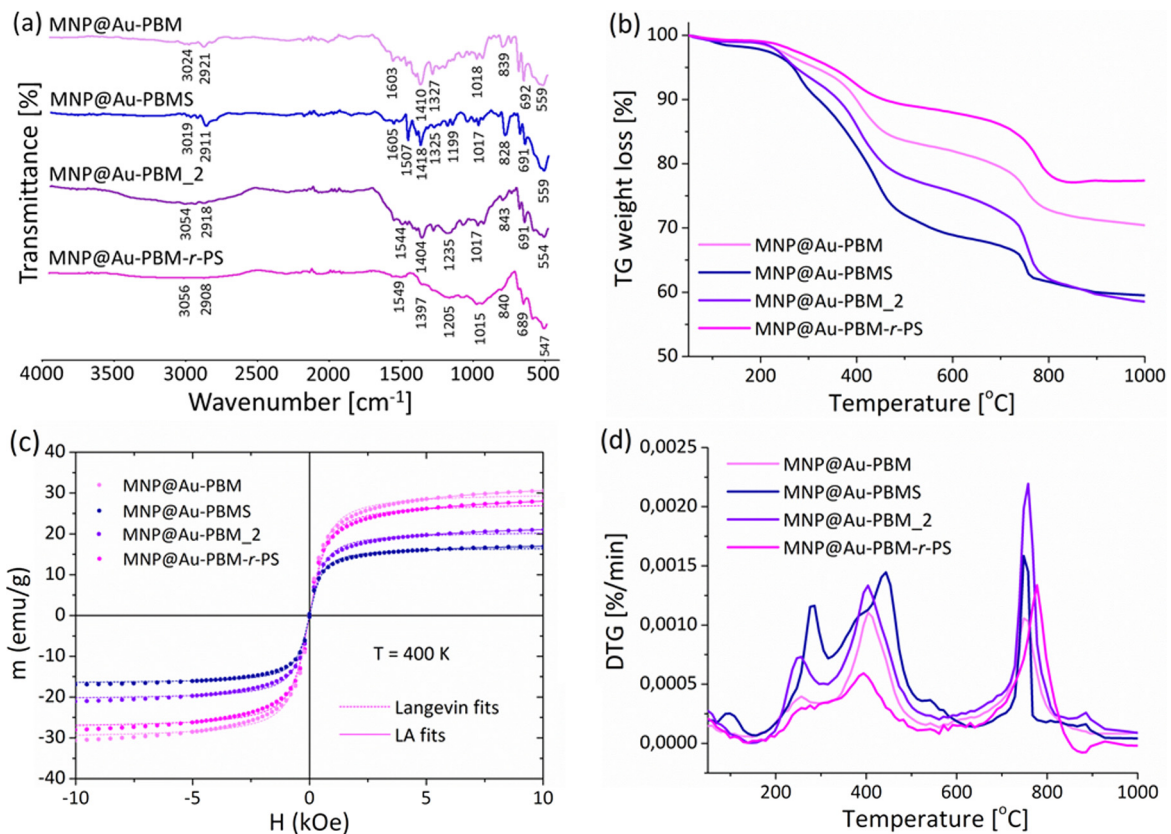


Figure 4 (a) ATR FT-IR spectra; (b) TGA curves; (c) magnetization as a function of external magnetic field measured at 400 K; and (d) DTG curves of polymer-coated MNP@Au.

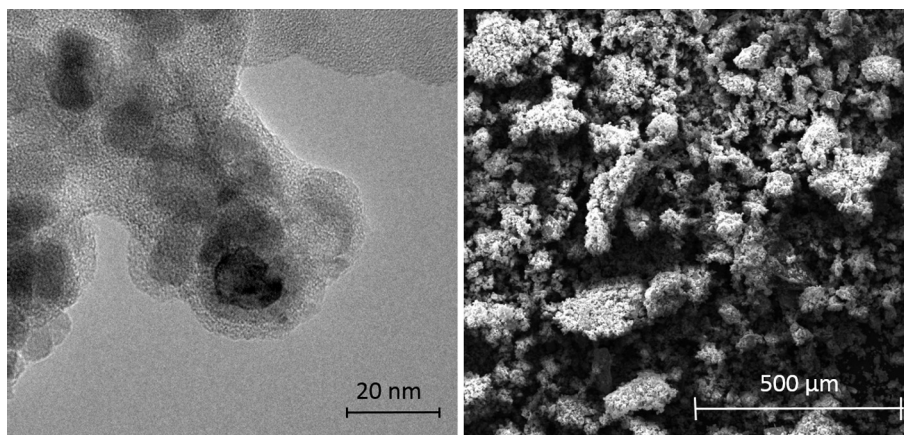


Figure 5 TEM and SEM images of MNP@Au-PBM nanoparticles.

This pathogen is responsible for increased morbidity and mortality of hospitalized patients (Wnorowska et al., 2015).

Fig. 6a shows that antibacterial effect of nanoparticles modified with PBM and PBMS against *P. aeruginosa* is much higher comparing to commercially available styrene. Additionally, the activity of MNP@Au-PBMS is 20% stronger than the activity of free monomer. Similar inhibitory effect (~80%) of *P. aeruginosa* growth was observed in the case of BM and MNP@Au-PBM. The decrease of *P. aeruginosa* Xen 5 chemiluminescence indicates the ability of nanohybrids to affect bac-

teria metabolism (Fig. 6b). Additionally, this effect reached up to 80% within ~60 s of treatment at dose 100 μg/ml and was observed for PBM and PBMS coated MNPs. Our recent report indicated that colistin which is an antibiotic mostly used for the treatment of lung infection in CF patients decreased the luminescence signal by ~24% at dose 100 μg/ml (Niemirowicz et al., 2015a). The formation of a biofilm is associated with increased resistance to an antibiotic treatment. It is established, that to kill bacteria cells embedded in biofilm matrix 1000 – fold dose of antibiotics are required. Moreover, data

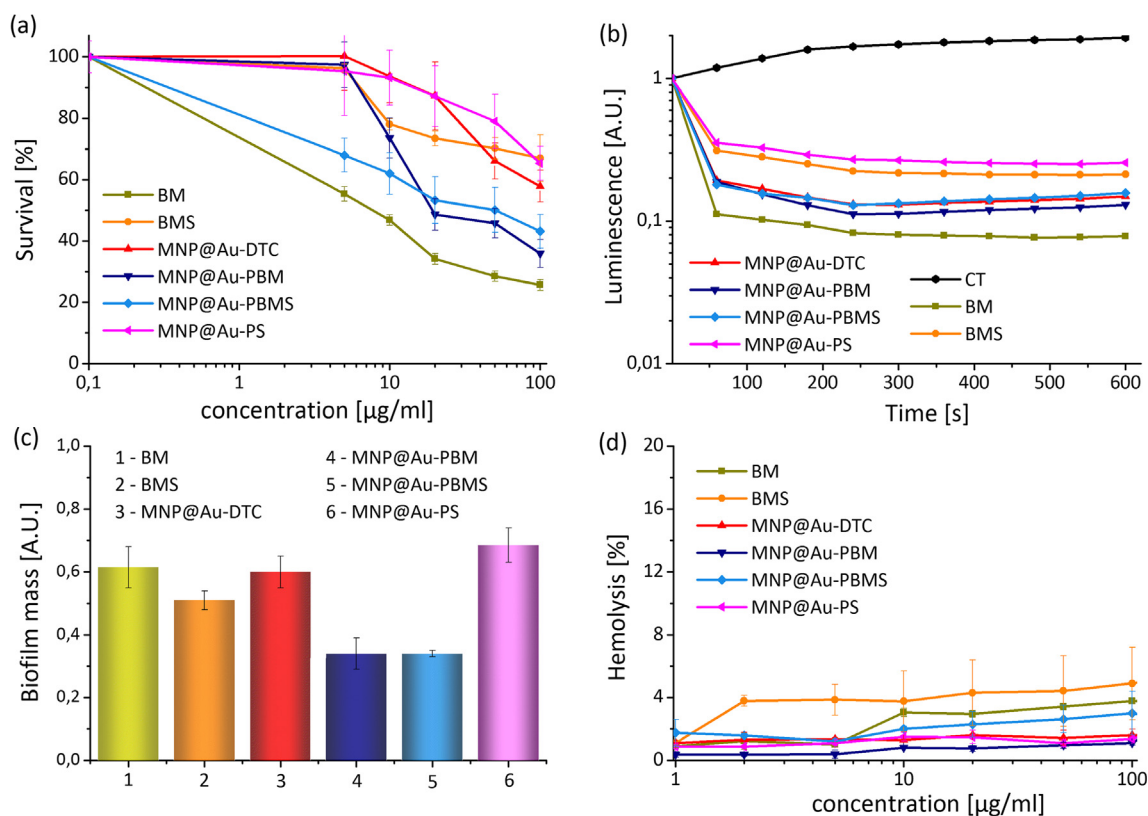
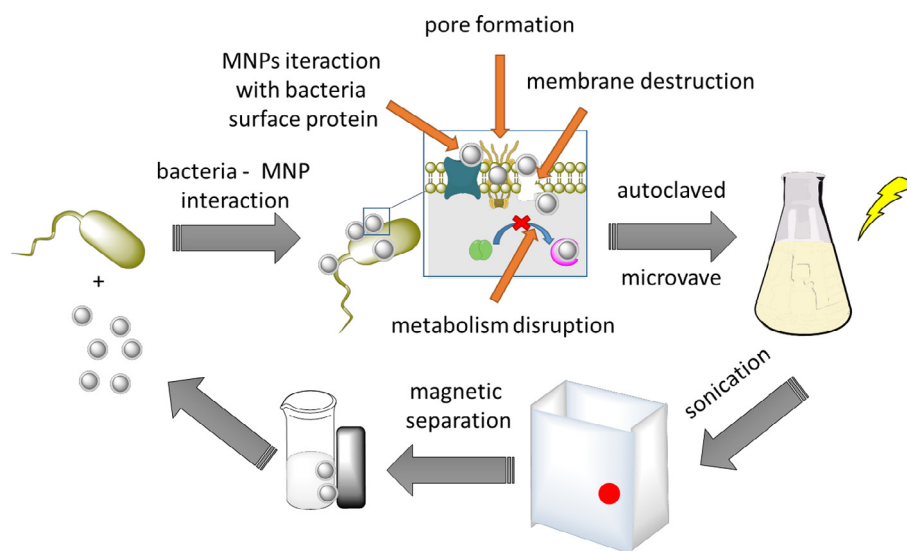


Figure 6 Biological properties of obtained materials: (a) bactericidal activity against *P. aeruginosa* strains; (b) reduction of *P. aeruginosa* chemiluminescence signal after MNP addition, (c) activity against bacteria biofilm formation and (d) hemocompatibility. CT - control sample – untreated *Pseudomonas aeruginosa* cells.



Scheme 3 Proposed mechanism of nanohybrids action and their regeneration.

show that biofilm plays a key role in chronic and recurrent *Pseudomonas* infections (Cantón et al., 2011; Cervia et al., 2009; de Bentzmann and Plésiat, 2011). Therefore, new strategies to prevent bacterial biofilm formation are a great challenge. As is indicated in Fig. 6c, MNP@Au-PBMS and MNP@Au-PBM are able to prevent biofilm formation and

effectively kill bacteria embedded into the biofilm matrix. Both nanohybrids at the concentration of 100 $\mu\text{g/ml}$ inhibited biofilm formation by $\sim 70\%$. It should be emphasized that this effect is twice stronger when compared to anti-biofilm properties of compounds in free forms. For MNP@Au-DTC and MNP@Au-PS the reduction in adhesion of *Pseudomonas*

aeruginosa was established around 40%, which indicated that the presence of polystyrene surface does not exert changes in anti-biofilm properties of tested nanohybrids. Our results show that PBM and PBMS coatings are useful to prevent bacteria biofilm formation and have stronger activity in comparison with previously described nanosystems (Webster et al., 2013). Leuba et al. indicated that bare MNPs and their derivatives coated with various functional groups such as amine, carboxyl and isocyanate are able to decrease the formation of biofilm; however, dose around 1 mg/mL is needed (Webster et al., 2013). Additionally, recently published data show that magnetic nanoparticles have a capability to penetrate biofilm (Hetrick et al., 2009; Sathyanarayanan et al., 2013). Park et al. presented that magnetic nanoparticles are able to inactivate pathogens in the presence of external magnetic field after induction of hyperthermia (Park et al., 2011). It is established that divalent cations such as Mg^{2+} are essential for biofilm formation (Cavaliere et al., 2014). The ability of PBM and PBMS to chelate divalent cations may explain their additional mechanism of action. Based on our results and published reports it is postulated that possible mechanism of action strongly depends on the nature of nanomaterial surface. It is likely that nanohybrids due to interaction with surface molecules which built bacteria cell wall, and ability to penetrate membranes and/or form pores, cause destruction of plasma membrane. In the next step they probably interfere the metabolic pathway in bacteria cells that lead to restriction of their growth. The proposed mechanism of nanohybrids action and their regeneration is presented in Scheme 3.

Several data revealed that there is a relationship between a particle type and a toxic effect which is observed during exposition (Choi et al., 2010; Kai et al., 2011). Additionally, a lot of reports demonstrated that cytotoxic effects commonly depend on basic physicochemical and morphological parameters of nanomaterials (Nagy et al., 2012; Sohaebuddin et al., 2010). Our recent results indicate that core-shell nanoparticles exert low hemolytic activity and low cytotoxic effect against host cells (Niemirowicz et al., 2015b, 2016; Car et al., 2014). In this study, data shown in Fig. 6d indicate that tested agents do not affect red blood cells membrane permeability at the concentration range of 1–100 $\mu\text{g}/\text{ml}$. However, at this concentration, PBM and PBMS coated MNP effectively kill and restrict metabolic activity of planktonic *P. aeruginosa* as well as prevent against bacteria biofilm formation.

4. Conclusion

In conclusion, new multifunctional polymer/gold/magnetic nanohybrids were synthesized and characterized by FT-IR, TEM, SEM and TG analyses. Control over properties of polymeric shell was achieved by surface-initiated RAFT/MADIX polymerization method. Commercially available and original bifunctional monomers based on thiosemicarbazide were used to form shells around gold-coated MNPs. Antibacterial properties of the obtained materials against *P. aeruginosa* were investigated. Bactericidal activity of free monomers and their polymer-magnetic nanohybrids were compared and the advantage of the latter ones was clearly proven. It was documented that tested agents at a low concentration effectively kill and restrict metabolic activity of planktonic *P. aeruginosa* as well as prevent against bacteria biofilm formation. Additionally, hemocompatibility tests carried out with the monomers alone and their polymer-magnetic hybrids revealed that the lysis rates observed with nanohybrids were lower than

for free monomers. Due to the superparamagnetic properties, there is a possibility to easily separate, purify and recycle these efficient antibacterial nanomaterials by application of an external magnetic field.

Acknowledgment

This work was financially supported by the National Science Centre, Poland, grant no. NCN/2014/13/N/ST5/01563. The equipment in the Center of Synthesis and Analysis BioNano-Techno of University of Białystok was funded by the EU as part of the Operational Program Development of Eastern Poland 2007–2013, project: POPW.01.03.00–20–034/09 and POPW.01.03.00–004/11.

Appendix A. Supplementary data

Supplementary data associated with this article can be found, in the online version, at <http://dx.doi.org/10.1016/j.arabjc.2016.12.014>.

References

- Abbas, M., Takahashi, M., Kim, C., 2013. Facile sonochemical synthesis of high-moment magnetite (Fe_3O_4) nanocube. *J. Nanopart. Res.* 15, 1354–1361. <http://dx.doi.org/10.1007/s11051-012-1354-y>.
- Ashkarran, A.A., Ghavami, M., Aghaverdi, H., Stroeve, P., Mahmoudi, M., 2012. Bacterial effects and protein corona evaluations: crucial ignored factors in the prediction of bio-efficacy of various forms of silver nanoparticles. *Chem. Res. Toxicol.* 25, 1231–1242. <http://dx.doi.org/10.1021/tx300083s>.
- Azam, A., 2012. Size-dependent antimicrobial properties of CuO nanoparticles against Gram-positive and -negative bacterial strains. *Int. J. Nanomed.* 3527–3535. <http://dx.doi.org/10.2147/IJN.S29020>.
- Azam, A., Ahmed, A.S., Oves, M., Khan, M.S., Habib, S.S., Memic, A., 2012. Antimicrobial activity of metal oxide nanoparticles against Gram-positive and Gram-negative bacteria: a comparative study. *Int. J. Nanomed.* 6003–6009. <http://dx.doi.org/10.2147/IJN.S35347>.
- Bain, C.D., Biebuyck, H.A., Whitesides, G.M., 1989. Comparison of self-assembled monolayers on gold: coadsorption of thiols and disulfides. *Langmuir* 5, 723–727. <http://dx.doi.org/10.1021/la00087a027>.
- Bankiewicz, B., Wojtulewski, S., Markiewicz, K.H., Wilczewska, A.Z., 2016. Carbamohydrazonothioate derivative—experimental and theoretical explorations of the crystal and molecular structure. *Struc. Chem.* <http://dx.doi.org/10.1007/s11224-016-0874-y>.
- Beija, M., Marty, J.-D., Destarac, M., 2011. RAFT/MADIX polymers for the preparation of polymer/inorganic nanohybrids. *Prog. Polym. Sci.* 36, 845–886. <http://dx.doi.org/10.1016/j.progpolymsci.2011.01.002>.
- Bharti, S., Neelam, Naqvi F., Azam, A., 2003. Synthesis, spectral studies and screening for amoebicidal activity of new palladium(II) complexes derived from thiophene-2-carboxaldehyde thiosemicarbazones. *Bioorg. Med. Chem. Lett.* 13, 689–692. [http://dx.doi.org/10.1016/S0960-894X\(02\)01005-3](http://dx.doi.org/10.1016/S0960-894X(02)01005-3).
- Cantón, R., Fernández Olmos, A., de la Pedrosa, E.G.G., Del Campo, R., Antonia Meseguer, M., 2011. Infección bronquial crónica: el problema de *Pseudomonas aeruginosa*. *Arch. Bronconeumol.* 47, 8–13. [http://dx.doi.org/10.1016/S0300-2896\(11\)70029-1](http://dx.doi.org/10.1016/S0300-2896(11)70029-1).
- Car, H., Niemirowicz, K., Swiecicka, I., Wilczewska, A., Bienias, K., Bucki, R., Misztalewska, I., Kalska-Szostko, B., 2014. Gold-functionalized magnetic nanoparticles restrict growth of *Pseu-*

- domonas aeruginosa*. Int. J. Nanomed. 2217–2224. <http://dx.doi.org/10.2147/IJN.S56588>.
- Cavaliere, R., Ball, J.L., Turnbull, L., Whitchurch, C.B., 2014. The biofilm matrix destabilizers, EDTA and DNaseI, enhance the susceptibility of nontypeable *Hemophilus influenzae* biofilms to treatment with ampicillin and ciprofloxacin. MicrobiologyOpen 3, 557–567. <http://dx.doi.org/10.1002/mbo3.187>.
- Cervia, J.S., Ortolano, G.A., Canonica, F.P., McAlister, M.B., 2009. Role of biofilm in *Pseudomonas aeruginosa* colonization and Infection. Infect. Control Hosp. Epidemiol. 30, 925–927. <http://dx.doi.org/10.1086/605643>.
- Choi, J.Y., Lee, S.H., Na, H.B., An, K., Hyeon, T., Seo, T.S., 2010. In vitro cytotoxicity screening of water-dispersible metal oxide nanoparticles in human cell lines. Bioprocess Biosyst. Eng. 33, 21–30. <http://dx.doi.org/10.1007/s00449-009-0354-5>.
- de Bentzmann, S., Plésiat, P., 2011. The *Pseudomonas aeruginosa* opportunistic pathogen and human infections: *Pseudomonas aeruginosa* and human infections. Environ. Microbiol. 13, 1655–1665. <http://dx.doi.org/10.1111/j.1462-2920.2011.02469.x>.
- Destarac, M., 2010. Controlled radical polymerization: industrial stakes, obstacles and achievements. Macromol. React. Eng. 4, 165–179. <http://dx.doi.org/10.1002/mren.200900087>.
- Destarac, M., Brochon, C., Catala, J.-M., Wilczewska, A., Zard, S.Z., 2002. Macromolecular design via the interchange of xanthates (MADIX): polymerization of styrene with O-ethyl xanthates as controlling agents. Macromol. Chem. Phys. 203, 2281–2289. <http://dx.doi.org/10.1002/macp.200290002>.
- Dong, H., Huang, J., Koepsel, R.R., Ye, P., Russell, A.J., Matyjaszewski, K., 2011. Recyclable antibacterial magnetic nanoparticles grafted with quaternized poly(2-(dimethylamino)ethyl methacrylate) brushes. Biomacromolecules 12, 1305–1311. <http://dx.doi.org/10.1021/bm200031v>.
- Fenter, P., Eberhardt, A., Eisenberger, P., 1994. Self-assembly of n-alkyl thiols as disulfides on Au(111). Science 266, 1216–1218. <http://dx.doi.org/10.1126/science.266.5188.1216>.
- Genova, P., Varadinova, T., Matesanz, A.I., Marinova, D., Souza, P., 2004. Toxic effects of bis(thiosemicarbazone) compounds and its palladium(II) complexes on herpes simplex virus growth. Toxicol. Appl. Pharmacol. 197, 107–112. <http://dx.doi.org/10.1016/j.taap.2004.02.006>.
- Guivar, J.A.R., Martinez, A.I., Anaya, A.O., Valladares, L.D.L.S., Félix, L.L., Dominguez, A.B., 2014. Structural and magnetic properties of monophasic maghemite nanocrystalline powder. Adv. Nanopart. 3, 114–121. <http://dx.doi.org/10.4236/anp.2014.33016>.
- Hajipour, M.J., Fromm, K.M., Akbar Ashkarran, A., Jimenez de Aberasturi, D., de Larramendi, I.R., Rojo, T., Serpooshan, V., Parak, W.J., Mahmoudi, M., 2012. Antibacterial properties of nanoparticles. Trends Biotechnol. 30, 499–511. <http://dx.doi.org/10.1016/j.tibtech.2012.06.004>.
- Hetrick, E.M., Shin, J.H., Paul, H.S., Schoenfisch, M.H., 2009. Antibiofilm efficacy of nitric oxide-releasing silica nanoparticles. Biomaterials 30, 2782–2789. <http://dx.doi.org/10.1016/j.biomaterials.2009.01.052>.
- Jafari, T., Simchi, A., Khakpash, N., 2010. Synthesis and cytotoxicity assessment of superparamagnetic iron–gold core–shell nanoparticles coated with polyglycerol. J. Colloid Interface Sci. 345, 64–71. <http://dx.doi.org/10.1016/j.jcis.2010.01.038>.
- Jiang, Q.-L., Zheng, S.W., Hong, R.Y., Deng, S.M., Guo, L., Hu, R.L., Gao, B., Huang, M., Cheng, L.F., Liu, G.H., Wang, Y.Q., 2014. Folic acid-conjugated Fe₃O₄ magnetic nanoparticles for hyperthermia and MRI in vitro and in vivo. Appl. Surf. Sci. 307, 224–233. <http://dx.doi.org/10.1016/j.apsusc.2014.04.018>.
- Kai, W., Xiaojun, X., Ximing, P., Zhenqing, H., Qiqing, Z., 2011. Cytotoxic effects and the mechanism of three types of magnetic nanoparticles on human hepatoma BEL-7402 cells. Nanoscale Res. Lett. 6 480 (1–10), 1. <http://dx.doi.org/10.1186/1556-276X-6-48>.
- Kainz, Q.M., Reiser, O., 2014. Polymer- and dendrimer-coated magnetic nanoparticles as versatile supports for catalysts, scavengers, and reagents. Acc. Chem. Res. 47, 667–677. <http://dx.doi.org/10.1021/ar400236y>.
- Kalska-Szostko, B., Satuła, D., Olszewski, W., 2015. Mössbauer spectroscopy studies of the magnetic properties of ferrite nanoparticles. Curr. Appl. Phys. 15, 226–231. <http://dx.doi.org/10.1016/j.cap.2014.12.011>.
- Kashevsky, B.E., Kashevsky, S.B., Korenkov, V.S., Istomin, Y.P., Terpinskaya, T.I., Ulashchik, V.S., 2015. Magnetic hyperthermia with hard-magnetic nanoparticles. J. Magn. Magn. Mater. 380, 335–340. <http://dx.doi.org/10.1016/j.jmmm.2014.10.109>.
- Lavrich, D.J., Wetterer, S.M., Bernasek, S.L., Scoles, G., 1998. Physisorption and chemisorption of alkanethiols and alkyl sulfides on Au(111). J. Phys. Chem. B 102, 3456–3465. <http://dx.doi.org/10.1021/jp980047v>.
- Lobana, T.S., Sharma, R., Bawa, G., Khanna, S., 2009. Bonding and structure trends of thiosemicarbazone derivatives of metals—An overview. Coord. Chem. Rev. 253, 977–1055. <http://dx.doi.org/10.1016/j.ccr.2008.07.004>.
- Mahadevan, S., Gnanaprakash, G., Philip, J., Rao, B.P.C., Jayakumar, T., 2007. X-ray diffraction-based characterization of magnetite nanoparticles in presence of goethite and correlation with magnetic properties. Phys. E Low-Dimens. Syst. Nanostruct. 39, 20–25. <http://dx.doi.org/10.1016/j.physe.2006.12.041>.
- Markiewicz, K.H., Miklasz, P., Poltorak, K., Misztalewska, I., Wojtulewski, S., Majcher, A., Fornal, E., Wilczewska, A.Z., 2016. Magnetic nanoparticles with chelating shells prepared by RAFT/MADIX polymerization. New J. Chem. 40, 9223–9231. <http://dx.doi.org/10.1039/C6NJ01938B>.
- Misztalewska, I., Wilczewska, A.Z., Wojtasik, O., Markiewicz, K.H., Kuchlewski, P., Majcher, A.M., 2015. New acetylacetonate-polymer modified nanoparticles as magnetically separable complexing agents. RSC Adv. 5, 100281–100289. <http://dx.doi.org/10.1039/C5RA20137C>.
- Moraes Silva, S., Tavallaie, R., Sandiford, L., Tilley, R.D., Gooding, J.J., 2016. Gold coated magnetic nanoparticles: from preparation to surface modification for analytical and biomedical applications. Chem. Commun. 52, 7528–7540. <http://dx.doi.org/10.1039/C6CC03225G>.
- Movahedi, Z., Pourakbari, B., Mahmoudi, S., Sabouni, F., Ashtiani Haghi, M.T., Hosseinpour Sadeghi, R., Mamishi, S., 2013. *Pseudomonas aeruginosa* infection among cystic fibrosis and ICU patients in the referral children medical hospital in Tehran. Iran 54, 24–28. <http://dx.doi.org/10.15167/2421-4248/jpmh2013.54.1.367>.
- Nagy, A., Steinbrück, A., Gao, J., Doggett, N., Hollingsworth, J.A., Iyer, R., 2012. Comprehensive analysis of the effects of CdSe quantum dot size, surface charge, and functionalization on primary human lung cells. ACS Nano 6, 4748–4762. <http://dx.doi.org/10.1021/nn204886b>.
- Niemirówic, K., Durnaś, B., Tokajuk, G., Głuszek, K., Wilczewska, A.Z., Misztalewska, I., Mystkowska, J., Michalak, G., Sodo, A., Wątek, M., Kiziewicz, B., Gózdź, S., Głuszek, S., Bucki, R., 2016. Magnetic nanoparticles as a drug delivery system that enhance fungicidal activity of polyene antibiotics. Nanomed. Nanotechnol. Biol. Med. 12, 2395–2404. <http://dx.doi.org/10.1016/j.nano.2016.07.006>.
- Niemirówic, K., Markiewicz, K., Wilczewska, A., Car, H., 2012. Magnetic nanoparticles as new diagnostic tools in medicine. Adv. Med. Sci. 57, 196–207. <http://dx.doi.org/10.2478/v10039-012-0031-9>.
- Niemirówic, K., Surel, U., Wilczewska, A.Z., Mystkowska, J., Piktel, E., Gu, X., Namiot, Z., Kułakowska, A., Savage, P.B., Bucki, R., 2015a. Bactericidal activity and biocompatibility of ceragenin-coated magnetic nanoparticles. J. Nanobiotechnol. 13, 1–11. <http://dx.doi.org/10.1186/s12951-015-0093-5>.
- Niemirówic, K., Swiecicka, I., Wilczewska, A.Z., Markiewicz, K.H., Surel, U., Kułakowska, A., Namiot, Z., Sznayka, B., Bucki, R., Car, H., 2015b. Growth arrest and rapid capture of select pathogens following magnetic nanoparticle treatment. Colloids

- Surf. B Biointerfaces 131, 29–38. <http://dx.doi.org/10.1016/j.colsurfb.2015.04.016>.
- Park, H., Park, H.-J., Kim, J.A., Lee, S.H., Kim, J.H., Yoon, J., Park, T.H., 2011. Inactivation of *Pseudomonas aeruginosa* PA01 biofilms by hyperthermia using superparamagnetic nanoparticles. J. Microbiol. Methods 84, 41–45. <http://dx.doi.org/10.1016/j.mimet.2010.10.010>.
- Perrier, S., Takolpuckdee, P., 2005. Macromolecular design via reversible addition-fragmentation chain transfer (RAFT)/xanthates (MADIX) polymerization. J. Polym. Sci. Part Polym. Chem. 43, 5347–5393. <http://dx.doi.org/10.1002/pola.20986>.
- Robinson, I., Tung, L.D., Maenosono, S., Wälti, C., Thanh, N.T.K., 2010. Synthesis of core-shell gold coated magnetic nanoparticles and their interaction with thiolated DNA. Nanoscale 2, 2624. <http://dx.doi.org/10.1039/c0nr00621a>.
- Rudolf, B., Salmann, M., Grobely, J., Celichowski, G., Tomaszewska, E., 2011. Synthesis and characterization of metallocarbonyl functionalized gold nanoparticles. Colloids Surf. Physicochem. Eng. Asp. 385, 241–248. <http://dx.doi.org/10.1016/j.colsurfa.2011.06.019>.
- Sankaraperumal, A., Karthikeyan, J., Shetty, A.N., Lakshmisundaram, R., 2013. Nickel(II) complex of p-[N, N-bis(2-chloroethyl) amino]benzaldehyde-4-methyl thiosemicarbazone: synthesis, structural characterization and biological application. Polyhedron 50, 264–269. <http://dx.doi.org/10.1016/j.poly.2012.11.006>.
- Sathyanarayanan, M.B., Balachandranath, R., Genji Srinivasulu, Y., Kannaiyan, S.K., Subbiahdoss, G., 2013. The effect of gold and iron-oxide nanoparticles on biofilm-forming pathogens. ISRN Microbiol. 2013, 1–5. <http://dx.doi.org/10.1155/2013/272086>.
- Sohaebuddin, S.K., Thevenot, P.T., Baker, D., Eaton, J.W., Tang, L., 2010. Nanomaterial cytotoxicity is composition, size, and cell type dependent. Part. Fibre Toxicol. 7 (22), 1–17. <http://dx.doi.org/10.1186/1743-8977-7-2>.
- Soykan, C., Erol, ?brahim, 2003. Synthesis, characterization, and biological activity of N-(4-acetylphenyl)maleimide and its oxime, carbazone, thiosemicarbazone derivatives and their polymers. J. Polym. Sci. Part Polym. Chem. 41, 1942–1951. <http://dx.doi.org/10.1002/pola.10738>.
- Tamer, U., Gündoğdu, Y., Boyacı, İ.H., Pekmez, K., 2010. Synthesis of magnetic core-shell Fe₃O₄-Au nanoparticle for biomolecule immobilization and detection. J. Nanopart. Res. 12, 1187–1196. <http://dx.doi.org/10.1007/s11051-009-9749-0>.
- Taton, D., Wilczewska, A.-Z., Destarac, M., 2001. Direct Synthesis of double hydrophilic statistical di- and triblock copolymers comprised of acrylamide and acrylic acid units via the MADIX process. Macromol. Rapid Commun. 22, 1497–1503. [http://dx.doi.org/10.1002/1521-3927\(20011201\)22:18 <1497::AID-MARC1497>3.0.CO;2-M](http://dx.doi.org/10.1002/1521-3927(20011201)22:18 <1497::AID-MARC1497>3.0.CO;2-M).
- Thomas Webster, T.J., 2010. Bactericidal effect of iron oxide nanoparticles on *Staphylococcus aureus*. Int. J. Nanomed. 277–283. <http://dx.doi.org/10.2147/IJN.S9220>.
- Ulman, A., 1996. Formation and structure of self-assembled monolayers. Chem. Rev. 96, 1533–1554. <http://dx.doi.org/10.1021/cr9502357>.
- Webster, T.J., Leuba, K., Durmus, Taylor, 2013. Short communication: carboxylate functionalized superparamagnetic iron oxide nanoparticles (SPION) for the reduction of *S. aureus* growth post biofilm formation. Int. J. Nanomed. 12, 731–736. <http://dx.doi.org/10.2147/IJN.S3825>.
- Webster, T.J., Seil, I., 2012. Antimicrobial applications of nanotechnology: methods and literature. Int. J. Nanomed. 2767–2781. <http://dx.doi.org/10.2147/IJN.S24805>.
- Webster, T.J., Taylor, 2011. Reducing infections through nanotechnology and nanoparticles. Int. J. Nanomed. 1463–1473. <http://dx.doi.org/10.2147/IJN.S22021>.
- Wilczewska, A.Z., Markiewicz, K.H., 2014. Surface-initiated RAFT/MADIX polymerization on xanthate-coated iron oxide nanoparticles. Macromol. Chem. Phys. 215, 190–197. <http://dx.doi.org/10.1002/macp.201300400>.
- Wilczewska, A.Z., Misztalewska, I., 2014. Direct synthesis of imidazolium salt on magnetic nanoparticles and its palladium complex application in the heck reaction. Organometallics 33, 5203–5208. <http://dx.doi.org/10.1021/om500507q>.
- Wilczewska, A.Z., Niemirowicz, K., Markiewicz, K.H., Car, H., 2012. Nanoparticles as drug delivery systems. Pharmacol. Rep. 2012, 1020–1037.
- Wnorowska, U., Niemirowicz, K., Myint, M., Diamond, S.L., Wróblewska, M., Savage, P.B., Janmey, P.A., Bucki, R., 2015. Bactericidal activities of cathelicidin LL-37 and select cationic lipids against the hypervirulent *Pseudomonas aeruginosa* strain LESB58. Antimicrob. Agents Chemother. 59, 3808–3815. <http://dx.doi.org/10.1128/AAC.00421-15>.
- Zhao, Y., Perrier, S., 2015. Reversible addition-fragmentation chain transfer polymerization from surfaces. In: Vana, P. (Ed.), Controlled Radical Polymerization at and from Solid Surfaces. Springer International Publishing, Cham, pp. 77–106.